Doubly charged silicon vacancy center, Si-N complexes, and photochromism in N and Si codoped diamond

B. G. Breeze,[1] C. J. Meara,[2,3] X. X. Wu,[1] C. P. Michaels,[1] R. Gupta,[1] P. L. Diggle,[4] M. W. Dale,[4] B. L. Cann,[4] T. Ardon,[5] U. F. S. D'Haenens-Johansson,[5] I. Friel,[6] M. J. Rayson,[2] P. R. Briddon,[2] J. P. Goss,[2] M. E. Newton,[1,3] and B. L. Green[1,*]

[1]*Department of Physics, University of Warwick, Coventry CV4 7AL, United Kingdom*
[2]*School of Engineering, Newcastle University, Newcastle upon Tyne NE1 7RU, United Kingdom*
[3]*EPSRC Centre for Doctoral Training in Diamond Science and Technology, University of Warwick, Coventry, CV4 7AL, United Kingdom*
[4]*De Beers Group Technology, Maidenhead, Berkshire SL6 6JW, United Kingdom*
[5]*Gemological Institute of America, 50 W 47th Street, New York, New York 10036, USA*
[6]*Element Six, Global Innovation Centre, Fermi Avenue, Didcot OX11 0QR, United Kingdom*

(Received 5 February 2020; revised manuscript received 31 March 2020; accepted 5 May 2020; published 21 May 2020)

Diamond samples containing silicon and nitrogen are shown to be heavily photochromic, with the dominant visible changes due to simultaneous change in total $SiV^{0/-}$ concentration. The photochromism treatment is not capable of creating or destroying SiV defects, and thus we infer the presence of the optically inactive SiV^{2-}. We measure spectroscopic signatures we attribute to substitutional silicon in diamond, and identify a silicon-vacancy complex decorated with a nearest-neighbor nitrogen SiVN, supported by theoretical calculations.

DOI: 10.1103/PhysRevB.101.184115

I. INTRODUCTION

Diamond, as with other wide-band-gap semiconductors, has recently attracted attention as a host for optically active point defects with potential applications in quantum communication [1], nanophotonics [2,3], and quantum information processing (QIP) [4]. In addition to the well-known nitrogen-vacancy (NV, where V denotes a vacancy henceforth) [5], the group-IV-vacancy centers (SiV [6–8], SnV [9], and PbV [10]) have recently emerged as potential candidates in QIP applications.

Unlike bulk nitrogen-doped diamond, where a significant effort stretching over decades has identified many nitrogen-related point defects [11,12], relatively little experimental study has been performed on high-quality single crystal diamond which is bulk doped with silicon. The only definitive assignments of optical centers to silicon are the well-known SiV^- [13–15] and SiV^0 [8,16,17]. Additionally, electron paramagnetic resonance (EPR) studies have identified $SiVH^0$ [18,19] and SiV_2H^0 [20], while a tentative assignment has been made to SiB^0 [21]. Density functional theory (DFT) studies of silicon-related point defects indicate that isolated substitutional silicon Si_s is stable though aggregates are energetically unfavorable [22]. Some silicon-related multivacancy, multi-hydrogen, nitrogen-related complexes are theoretically stable [22,23] but most have yet to be identified experimentally.

In this work we have studied silicon and nitrogen codoped single-crystal synthetic diamond from as-grown to a treatment temperature of 2400 °C using a combination of optical absorption spectroscopies and EPR. We identify the neutrally charged silicon-vacancy-nitrogen complex $SiVN^0$ through combined experimental measurements and theoretical modeling, and tentatively assign an infrared absorption mode at 1338 cm^{-1} to substitutional silicon.

II. CHARGE TRANSFER

It is well established that as an insulator, defects in diamond may exist in more than one charge state in the same crystal simultaneously. For charge states which are dominated by the charge dynamics of nitrogen donors (the dominant impurity in the majority of synthetic diamond), a "charge transfer" protocol has been established to drive between the two extremal states [16,24,25]. Above-band-gap UV excitation ($\lambda < 225$ nm) of a sample typically maximizes the concentration of nitrogen donors N_s^0, which in turn tends to favor the neutral charge state of other defects. Heating the sample at 550 °C in the absence of light enables thermal excitation of electrons/holes, reversing the process and yielding N_s^+ while typically maximizing the concentrations of negatively charged versions of defects present. This has been previously demonstrated in several defects including SiV [16], NV [26], NVH [24], N_2V [27], and N_3V [28].

This charge instability can be a great advantage when studying fundamental defect properties as it enables multiple charge states of the same defect to be studied in the same crystal. In a single-electron charge transfer process (e.g., X^0 to X^- rather than X^+ to X^- for a given defect X), we expect at least one of the charge states to be EPR active. EPR is capable of absolutely quantifying the concentration of a defect and is

*Corresponding author: b.green@warwick.ac.uk

TABLE I. Summary of the samples employed in this study. All post-growth anneals were performed under stabilizing pressure and for 1 h, except for sample G which was annealed for 100 h. Dopants without explicit isotopes are natural abundance.

Sample	Dopants	Growth run	Annealing temp (°C)
A	^{15}N, Si	1	As-grown
B	^{15}N, Si	1	1600
C	^{15}N, Si	1	1800
D	^{15}N, Si	1	2000
E	^{15}N, Si	1	2200
F	^{15}N, Si	1	2400
G	N, Si	2	1800

therefore fundamentally the source of the optical absorption cross-section values for most defects in diamond [29]. Where charge transfer is present, the loss (gain) of the EPR-active charge state can be equated to the gain (loss) in the other, allowing an optical absorption cross section to be extracted for the non-EPR-active state. The major assumption made in the above procedure is that there are only two charge states of the defect accessible through the charge transfer protocol, and therefore the loss of one must equal the gain in the other. If this is not the case, and some charge population is lost to a third charge state, then an incorrect optical absorption cross section for the non-EPR-accessible charge state will be extracted.

III. EXPERIMENTAL DETAIL

A. Method and samples

Seven samples were grown in a microwave-plasma chemical vapor deposition (CVD) reactor: Samples A–F were grown simultaneously and doped with natural abundance silicon (via the addition of silane to the growth gases) and 100% ^{15}N-enriched nitrogen; sample G was doped with natural abundance silicon and nitrogen (Table I). Secondary ion mass spectrometry measurements on samples grown in the same conditions indicated $[N_s] = 9(2)$ ppm through the bulk, and a silicon incorporation uniformity to ±10%: we were unable to quantify the silicon due to the lack of a suitable reference sample. Growth substrates (all {0 0 1}-oriented) and nondiamond material were removed from all samples post-growth to leave free-standing plates. Samples B–F were each subsequently annealed under stabilizing pressure (6–8 GPa) for 1 h at 1600, 1800, …, 2400 °C, respectively: each sample was annealed only once (i.e., sample D was annealed at 2000 °C only). Sample G was annealed at 1800 °C for 100 h under stabilizing pressure. All samples were polished post-anneal to remove any etched or graphitic material and provide parallel, low-roughness faces for optical measurements. Each sample was approximately 3 × 3 × 1.6 mm.

As a consequence of the charge transfer effect (Sec. II), the annealing behavior of a given defect can be confused with its charge transfer properties if care is not taken to initialize the crystal to a known state before each measurement. We therefore perform all measurements immediately following either UV exposure (the "UV state") or heating in the dark at 550 °C for 20 min (the "heated state"): the sample is kept in the dark between treatment and measurement. For the UV state, samples were exposed using the xenon arc lamp of a DiamondView instrument for 6 min per face; heating was performed under a dry nitrogen atmosphere in a tube furnace (Elite Thermal Systems Ltd.) for 20 min at 550 °C. EPR measurements were performed at *X* band using a Bruker EMX-E spectrometer with 90 dB attenuator to avoid microwave power saturation, and ER4122SHQ resonator. EPR measurements were quantified by comparison to a standard reference sample containing 270 ppm N_s^0 and were performed below microwave power saturation. Ultraviolet-visible (UV-vis) and IR absorption measurements were performed in PerkinElmer Lambda 1050 and Spectrum GX spectrometers, respectively.

B. Computational method

Density functional theory within the supercell approach was employed using the AIMPRO software package [30]. We have used a generalized gradient approximation (GGA) [31] for the exchange and correlation and the pseudopotential approximation [32] to remove the core electrons from explicit determination. Kohn-Sham functions were expanded in a basis of atom-centered Gaussian functions [22] using four *d*-type functions resulting in 40 functions per atom. The charge density was Fourier transformed using plane waves with a cutoff of 300 Ha, which results in total energy convergence to 1×10^{-5} eV with respect to this parameter. The Brillouin zone was sampled using the Monkhorst-Pack scheme [33]: the maximum reciprocal volume per sampling point was 0.01.

Using this approach, the lattice constant of diamond agrees with experiment (3.57 Å [34]) to within 1%. All defect structures were modeled using simple-cubic supercells based upon the eight-atom conventional unit cell, with lattice spacing of $4a_0$ containing 512 atoms.

Donor and acceptor levels were found using the formation energy method [35,36], with the formation energy (E^f) for a certain charge state q, obtained using

$$E^f(X,q) = E_{\rm tot}(X,q) - \sum \mu_i + q\left(E_V^X + \mu_e\right) + \chi(X,q). \quad (1)$$

Here $E_{\rm tot}$ is the total energy of a defect structure, E_V^X is taken as the valence-band maximum, μ_e is the electron chemical potential, and χ is a correction term for periodic charge in the supercell [37]. χ comprised of a background electrostatic correction of meV order and the Madelung term for the $4a_0$ supercell calculated at 0.26 q^2 eV. Binding energies were calculated using formation energies [35,38], as the energy released in the formation of the complex from the component parts. Hyperfine tensor principal values and directions were determined as described previously [22,39].

IV. RESULTS

A. Annealing

Initially we consider the annealing study performed on the samples which were grown simultaneously (samples A–F). Each sample was initialized into the UV state and measured by IR and EPR to quantify the defects present—see Table II for details on quantification method for each defect.

TABLE II. Details and references for techniques and absorption cross-section coefficients employed in the quantification of defects at each annealing stage.

Defect	Technique	Note	Ref.
N_s^0	IR	1344 cm^{-1}	[40]
N_s^+	IR	1332 cm^{-1}	[41]
NVH^0	IR	3123 cm^{-1}	[42]
NVH^-	EPR		[43]
N_2VH^0	EPR		[44]
N_3VH^0	IR	3107 cm^{-1}	[44]
SiV^0	EPR		[16]
SiV^-	UV-vis	737 nm	[16]
$SiVN^0$	EPR	this work	

Sample A is dominated by nitrogen-related complexes, with the most abundant identified defects being $N_s^{0/+}$ and $NVH^{0/-}$ (Fig. 1). The only identified silicon-related centers are $SiV^{0/-}$ which are present at approximately 100 ppb combined. Any concentrations of $SiVH^0$ [19] and SiV_2H^0 [20] are below EPR detection limits (≈1 ppb). Sample A is visually brown but heavily photo/thermochromic, varying from deep brown to brown-pink in the UV and heated states, respectively.

Analogous to the well-known aggregation of nitrogen-vacancy centers in diamond (N_nV, where $n = 1$–4) [45], we observe the aggregation of N_nVH as the annealing temperature increases. A decrease in NVH at ⩾1800 °C and above is accompanied by an increase in N_2VH^0, which in turn decreases at 2400 °C with a corresponding rise in N_3VH^0 (Fig 1).

The majority of the sharp IR one-phonon and C-H stretch absorption peaks observed in sample A [Fig. 2(a)] have been

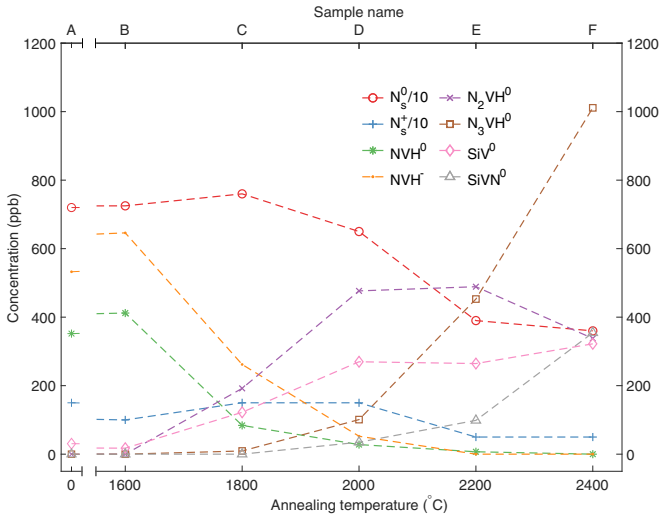

FIG. 1. Point defect concentrations measured by EPR and IR in samples grown simultaneously and subsequently annealed for 1 h at high temperature under stabilizing pressure (see Table I). All measurements taken with the sample in the UV-treated charge state (see text for details). Dashed lines are guides to the eye. Note that $N_s^{0/+}$ concentrations have been divided by 10 to increase legibility.

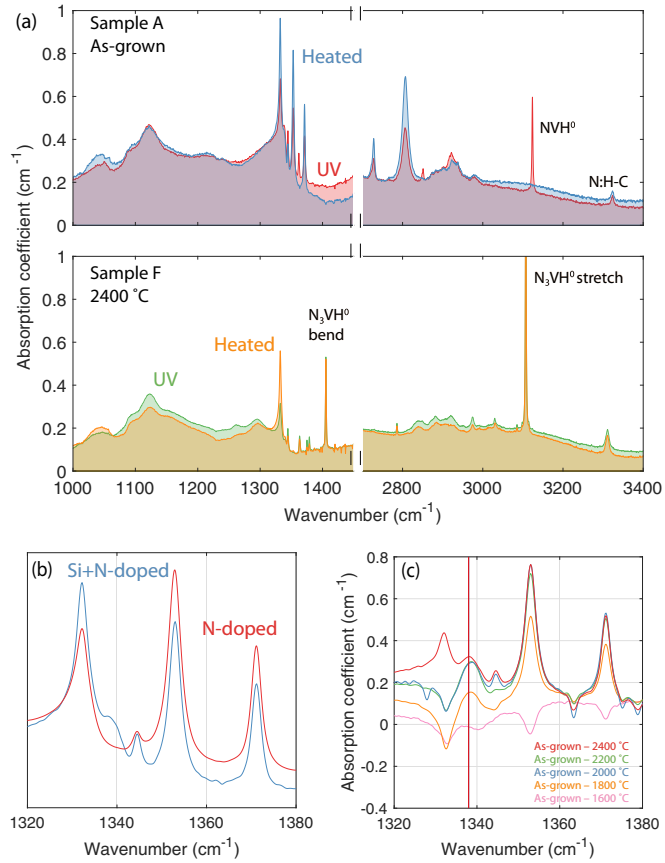

FIG. 2. (a) IR absorption spectra of sample A (top) and sample F (bottom) in the two extremal charge states. The two regions give the defect-induced one-phonon absorption (left) and C-H stretch region (right): the intrinsic multiphonon absorption has been subtracted. (b) The one phonon of two as-grown samples grown under similar CVD conditions: both are nitrogen doped but silicon was added to the growth gasses of one. The primary difference is the feature at approximately 1340 cm^{-1} in the silicon-containing sample, which is tentatively assigned to substitutional silicon [22]. The remaining peaks are reported in studies of solely nitrogen-doped CVD material [24]. (c) Difference spectra between sample A (as-grown) and samples treated at the given temperatures. The change in the 1338 cm^{-1} mode is highlighted.

previously observed in high-nitrogen, high-hydrogen brown diamond from several sources [46,47], and their photochromic behavior reported [47]. The point defect origin of these peaks has not been identified, but they do not appear to require silicon. However, the small shoulder at 1338 cm^{-1} is not present in previous reports of high-nitrogen material. The peak itself is not photochromic, and its frequency does not depend on nitrogen isotope. Samples grown under similar conditions but without the addition of silicon to the growth gasses produce similar one-phonon spectra except for the absence of the 1338 cm^{-1} mode [Fig. 2(b)]. Previous DFT calculations predict a mode originating at the carbon atoms surrounding substitutional silicon at 1333 cm^{-1} [22]: in conjunction with studies of silicon-doped HPHT-grown samples [48,49], we tentatively assign the 1338 cm^{-1} peak to substitutional silicon. Difference spectra reveal essentially no change between the as-grown and 1600 °C samples, with subsequent anneals

reducing the strength of the 1338 cm^{-1} mode [Fig. 2(c)]—this is consistent with the increase in observed Si-related defects from sample A to sample F (Fig 1).

The concentration of $SiV^{0/-}$ increases by over an order of magnitude from sample A to sample F. We conclude that the majority of the silicon was originally incorporated in other forms (assumedly substitutionally) during growth, with the subsequent production of SiV proceeding by vacancy capture during the HPHT treatment, analogous to the production of the N_nVH defects. EPR measurements of samples annealed at 2000 °C and higher reveal the presence of a previously unidentified silicon-containing defect. We identify this defect as a silicon-vacancy center decorated with a nitrogen atom ($SiVN^0$): the defect is discussed further in Sec. V. The concentration of SiV^0 and $SiVN^0$ measured in sample F (Fig. 1) indicates that at least 1 ppm of silicon must have been incorporated during growth.

Between samples A and F, approximately 4.5 ppm of substitutional nitrogen has been lost in addition to 1 ppm of $NVH^{0/-}$, and is accompanied by the production of approximately 0.3 and 1.0 ppm of N_2VH^0 and N_3VH^0, respectively. Together with $SiVN^0$ this corresponds to a total of 4.0 ppm nitrogen, accounting for the majority of the lost $N_s^{0/+}$ and NVH^{0-}. However, a significant concentration of nitrogen-related defects remain unidentified. As N_3VH contains three nitrogen atoms, a small error in its oscillator strength would have a dramatic effect on our ability to quantify total nitrogen in the high-temperature annealed samples.

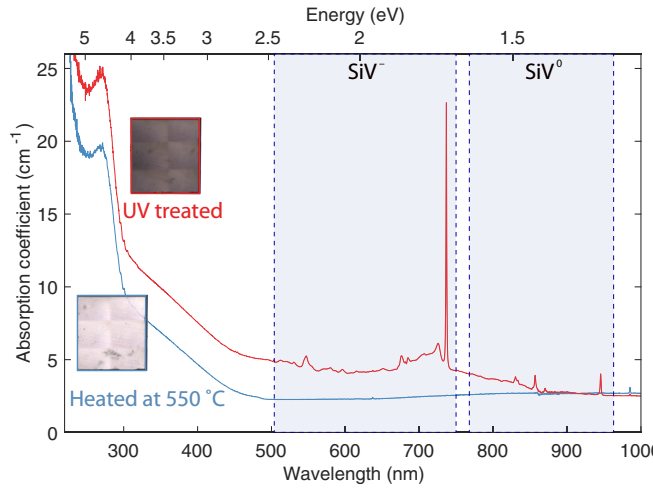

FIG. 3. UV-vis absorption spectra of sample D (annealed at 2000 °C) measured at 80 K in two extremal charge states—see text for details. Strong SiV^- and SiV^0 spectra are recorded in the UV-treated charge state, and are undetectable in the heated charge state. The charge transfer processes are reversible, i.e., no net SiV is created or destroyed in during the treatments: the dramatic loss of SiV^- and SiV^0 between extremal states is therefore strong evidence for the existence of a third charge state of SiV, which we identify as SiV^{2-} . Note that a broad SiV^0 absorption continues beneath the SiV^- absorption, but the structure between 500–740 nm belongs to SiV^- . Inset: Representative transmission images of the sample in the two extremal charge states.

B. Photochromism and evidence for SiV^{2-}

In previous studies of nitrogen-doped brown CVD diamond, samples which were annealed above 1600 °C became less brown, with higher temperatures corresponding to a greater reduction of brown color [24,25,50]. The present samples display the same behavior, with samples E and F (2200 and 2400 °C, respectively) appearing near colorless by eye in the heated state. Contrary to previous studies, the present samples treated at >2000 °C remain heavily photochromic, varying from a deep gray-blue to near colorless in the UV and heated states, respectively.

UV-vis measurements of sample D in the UV state show strong absorption from both SiV^- (737 nm) and SiV^0 (946 nm) (Fig. 3). The spectrum of the former reveals the optical structure associated with the second excited state of SiV^- [14,51] which has been reported previously in photoluminescence excitation [52,53]. Comparison of the absorption spectra in the UV and heated states confirms that the photo/thermochromism is dominated by dramatic changes in the concentration of SiV^- and SiV^0 (Fig. 3): this is the case for samples A–F. The visible photochromic color change in the present samples is much more extreme than the color change reported in nitrogen-doped CVD samples [24] due to the incredibly broad absorption band of SiV^0 compared to the relatively broad and weak absorption bands associated with NVH in purely nitrogen-doped material (Fig. 3).

The processes employed during the charge transfer procedure are not capable of destroying or creating SiV and we conclude that we are efficiently driving to a third charge state of SiV. The photochromic behavior of the samples is consistent with driving to a negatively (rather than positively) charged state. DFT studies of SiV predict that SiV^{2-} is a stable and electronically saturated system with no internal optical transitions or accessible spin levels and is thus difficult to spectroscopically observe [54]. We therefore infer the presence of SiV^{2-} by the absence of SiV^- and SiV^0 in the heated charge state.

C. Discussion

Doubly charged defects are well characterized in other group-IV semiconductors (e.g., Si [55,56] and Ge [57,58]) but have not been previously reported in diamond despite several theoretical predictions [23,59,60]. Generally this is a result of the paucity of very shallow donors and acceptor states in diamond, which are required to stabilize the chemical potential suitably for these doubly charged states (in the absence of negative-U effects [61]). However, in SiV the $(2-/-)$ transition is relatively deep (approximately midgap [54]), yielding a stable charge state even for deep nitrogen donors (at approximately $E_C - 1.7$ eV [62]).

Despite its lack of internal transitions, we still expect transitions from the SiV^{2-} ground state to the conduction band, which are theoretically predicted at ≈4 eV [54]. As a defect-to-band transition, this will manifest as spectrally broad rather than a sharp transition. There is a small change in the absorption gradient <250 nm (<5 eV) between the UV and heated states, but any absorption in this region is dominated by N_s^0 absorption (Fig. 3) [63] and hence difficult to isolate.

TABLE III. Spin Hamiltonian parameters measured for $SiVN^0$. The three principal values (p_{1-3}) and directions are given for each parameter. A positive tilt is given to mean away from [[0 0 $\bar{1}$]] toward [1 1 0]: no tilt is required for the final principal value of each parameter, retaining the [1 $\bar{1}$ 0] mirror plane and reflecting the defect's C_{1h} symmetry.

Parameter	Unit		p_1	Dir.	Tilt (deg)	p_2	Dir.	Tilt (deg)	p_3	Dir.
g	1	Expt.	2.00472 ± 0.00005	[0 0 $\bar{1}$]	+4.3	2.00549 ± 0.00005	[1 1 0]	+4.3	2.00288 ± 0.00005	[1 $\bar{1}$ 0]
A (^{14}N)	MHz	Expt.	-3.80 ± 0.01	[1 1 1]	+2.7	-3.59 ± 0.01	[1 1 $\bar{2}$]	+2.7	-3.28 ± 0.01	[1 $\bar{1}$ 0]
		Theory	−3.4	[1 1 1]	+6	−3.0	[1 1 $\bar{2}$]	+2	−2.7	[1 $\bar{1}$ 0]
Q (^{14}N)	MHz	Expt.	-2.08 ± 0.01	[1 1 1]	0	$+1.04 \pm 0.01$	[1 1 $\bar{2}$]	0	$+1.04 \pm 0.01$	[1 $\bar{1}$ 0]
A (^{29}Si)	MHz	Expt.	$\pm 98.24 \pm 0.5$	[2 2 $\bar{1}$]	0	$\pm 98.13 \pm 0.5$	[1 1 4]	0	$\pm 94.47 \pm 0.5$	[1 $\bar{1}$ 0]
		Theory	+87	[2 2 $\bar{1}$]	8	+89	[1 1 4]	8	+92	[1 $\bar{1}$ 0]

In sample D we measure the UV state concentrations of SiV^- and SiV^0 as 110 and 380 ppb, respectively (Fig. 3), using the conversion factors given in [16]: in the heated state the concentration of both charge states is below 1 ppb and therefore all SiV defects are in the 2− charge state, requiring 870 ppb of donor charges between the two states. The corresponding loss in N_s^0 from UV to heated states is 2.3 ppm, more than accounting for the SiV-related charge effects. This relationship is true at all annealing temperatures. As a result, the changes in donor concentrations cannot be attributed solely to SiV and it is therefore difficult to quantify the latent SiV^{2-} concentration in the UV state. Upper limits can be estimated based on the assumption that the only donor is N_s^0; however, this is known not to be the case in these samples (e.g., NVH^-, other photochromic peaks in Fig. 2).

The extremal charge states are unstable at room temperature in all of the present samples. Time-lapse absorption measurements of SiV^-, performed in the absence of ambient light, show that after UV treatment of sample F the concentration of SiV^- increases by approximately 70% over 9 h. Ambient light increases the rate of this change, and significant color changes are visible after 2 h in ambient. The changes cannot be described by a simple coupled model with constant leakage rates from $SiV^0 \rightarrow SiV^-$ and $SiV^- \rightarrow SiV^{2-}$. Instead, the increase is well described by a hyperbolic function, as expected by multiple overlapping thermal processes. This is consistent with the present material containing multiple thermally activated donors/acceptors at room temperature.

The existence of SiV^{2-} casts doubt on the optical absorption cross section for SiV^- given in [16]. The cross section for SiV^0 was calibrated by directly measuring its concentration by EPR and equating it to the absorption strength measured by UV-vis. However, the cross section for SiV^- was calibrated via charge transfer between SiV^0 and SiV^- using the protocol given in Sec. II: the loss of the former was equated to the gain in the latter. The assumption was that only two charge states were involved in the process: any loss or gain of population to or from SiV^{2-} was unaccounted for, and would result in a modified absorption cross section than the one given in [16]. The concentrations of SiV^- given by the cross section are within approximately a factor of 2 of the expected concentration based on charge balance arguments. However, the potentially high concentration of SiV^{2-} in these samples makes a more precise statement impossible at this time. A future study based on intrinsic or even p-type material should bias between SiV^- and SiV^0, allowing both present charge states to be quantified simultaneously and reliably. We note that even with the present uncertainty, our results remain incompatible with the 1×10^{-13} meV cm^{-2} value derived from first-principles calculations [64].

V. THE SILICON-VACANCY-NITROGEN DEFECT

A. Defect identification

The spin Hamiltonian for a single electron, multiple nucleus system is given by

$$\mathbf{H} = \mu_B \mathbf{B}^T \cdot \underline{\mathbf{g}} \cdot \mathbf{S} + \sum_i^N \mathbf{S}^T \cdot \underline{\mathbf{A}}_i \cdot \mathbf{I}_i + \mathbf{I}_i^T \cdot \underline{\mathbf{Q}}_i \cdot \mathbf{I}_i,$$

with i summed over the nuclei. These terms represent the electronic Zeeman, electron-nuclear hyperfine, and nuclear quadrupole interactions, respectively. Application of magnetic field lifts the degeneracy of the electronic states m_S via the Zeeman interaction, with transitions between the states driven by high frequency (typically microwave) magnetic fields—the electron paramagnetic resonance phenomenon. Each nucleus splits the electron resonance line into $2I + 1$ lines, where I is the nuclear spin of the isotope in question [1 (0) for ^{14}N (^{15}N) and 0 (1/2) for ^{28}Si (^{29}Si) respectively]. The quadrupole interaction (characterized by the tensor $\mathbf{Q}$) is nonzero only for nuclei with $I \geqslant 1$.

EPR measurements of samples D–F reveal a previously unidentified multiline $S = 1/2$ spectrum at approximately $g = 2.004$ [Fig. 4(a)]. Initial investigations indicated that spectrum can be accurately simulated using a spin Hamiltonian of a monoclinic C_{1h} defect which possesses a 100% $I = 1/2$ nucleus with a small hyperfine interaction. With the external magnetic field $B \| \langle 1\,1\,1 \rangle$, a C_{1h} defect (principal axis $\langle 1\,1\,0 \rangle$) possesses three inequivalent orientation sets with relative populations 1:1:2. Each population further has its electronic resonance split by interaction with the $I = 1/2$ nucleus, yielding the three orientation classes highlighted in [Fig. 4(a)].

As samples A–F are ^{15}N enriched, the nucleus involved could either be ^{15}N or ^{1}H. An additional sample, sample G, was grown under similar conditions to samples A–F but with natural abundance nitrogen rather than ^{15}N-enriched gasses and subsequently annealed at 1800 °C for 100 h. EPR measurements of sample G again exhibit a previously unidentified multiline $S = 1/2$ spectrum at approximately $g = 2.004$ but the spectrum is significantly more complex than in the ^{15}N-doped samples [Fig. 4(b)]. This spectral change under

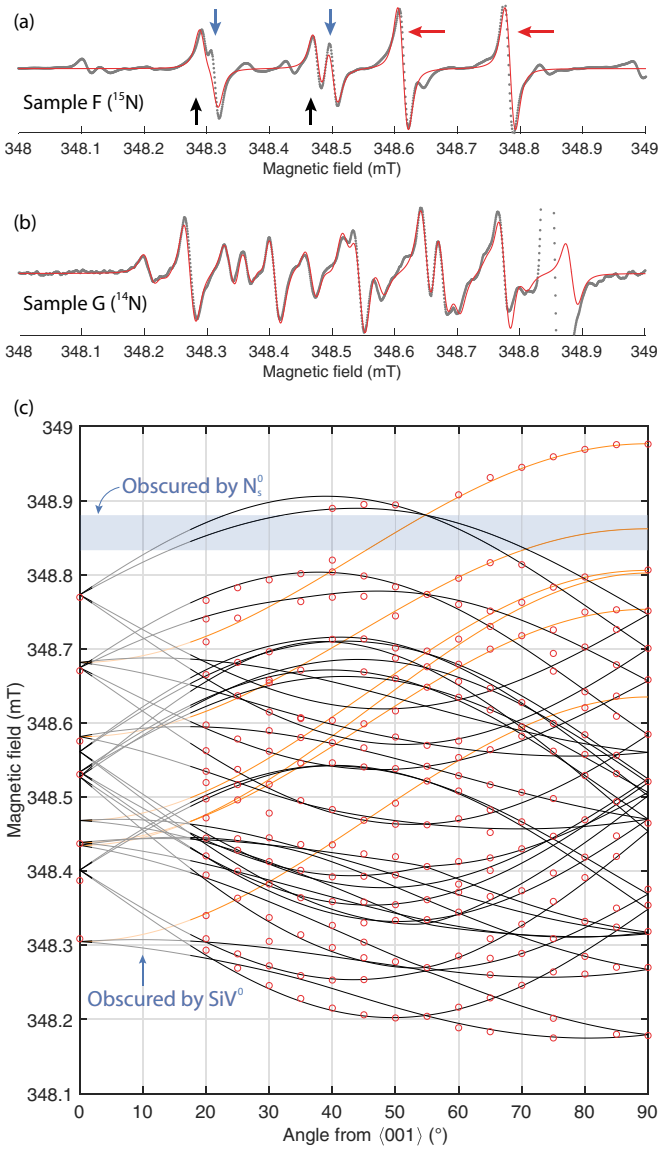

FIG. 4. EPR spectra of (a) sample F (^{15}N doped) and (b) sample G (^{14}N doped) with $B \| \langle 1\,1\,1 \rangle$. Experiment in black; simulation in red. Additional resonances in (a) are due to $^{15}N_2VH^0$. Arrows highlight resonances of the three inequivalent orientations of a C_{1h} defect (relative populations 1:1:2), each of which is split by interaction with an $I = 1/2$ ^{15}N nucleus. (c) Angular variation ($\{1\,1\,0\}$ plane) of measured EPR transition fields in sample G (circles) overlaid with a spin Hamiltonian simulation (Table III). Transitions of a single $SiVN^0$ orientation are highlighted to demonstrate the effect of the similar magnitude quadrupole and hyperfine interactions ($\Delta m_S = \pm 1$; $\Delta m_I = \pm 1$ transitions gain appreciable intensity) resulting in six transitions per orientation rather than the expected three.

nitrogen isotope change confirms the presence of nitrogen at the defect. Due to the isotopic abundances we identify this nucleus as a single nitrogen atom, eliminating hydrogen as a possibility.

The angular variation of the spectrum [Fig. 4(c)] confirms that it belongs to a defect possessing monoclinic C_{1h} symmetry and a small hyperfine interaction with the nitrogen (Table III), indicating essentially zero unpaired electron spin

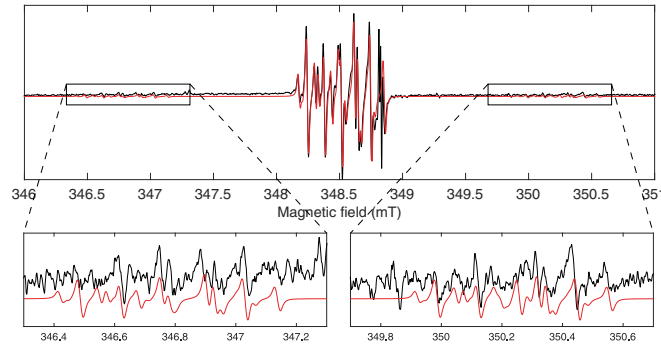

FIG. 5. EPR spectrum of sample G with $B \| \langle 1\,1\,1 \rangle$. Experimental data in black; simulation in red. Additional panels show the ^{29}Si hyperfines on each side of the primary spectrum. As expected, their intensity is 5% of the primary spectrum. Simulation generated by EasySpin [71] using the spin Hamiltonian parameters given in Table III.

density on the nitrogen nucleus [65]. The similar magnitude of the quadrupole and hyperfine interactions allows "forbidden" transitions ($\Delta m_S = \pm 1$; $\Delta m_I \neq 0$) to acquire appreciable intensity, yielding more than three transitions per orientation and significantly increasing the complexity of the spectrum [Fig. 4(c)]. This effect is observed in other nitrogen-related defects in diamond [28,65].

A large number of purely nitrogen-related defects have been identified by EPR in diamond, including N_s^0 [66], NV^- [67,68], interstitial nitrogen [69], and even substitutional nitrogen pairs [70]. It is thus unlikely that a new defect which involves only nitrogen would be identified in material which is novel due to its simultaneously high concentration of nitrogen and silicon. Therefore, we hypothesize that this defect must also contain silicon, whose 95% natural abundance of ^{28}Si ($I = 0$) makes it difficult to identify without a high defect concentration.

A previous DFT study into silicon-containing defects in diamond identified SiVN as a simple and stable defect candidate in high-nitrogen high-silicon diamond [22]. DFT calculations of the hyperfine parameters of the silicon and nitrogen in $SiVN^0$ (improving on previously-reported values [22]) were used as a guide for experimental parameters (Table III). To confirm the presence of silicon in the defect, long-term scans designed to increase the signal-to-noise enough to easily identify any ^{29}Si-related spectrum (approximately 5% of the natural abundance of ^{28}Si) were performed. These scans measured approximate replicas of the primary spectrum split by a nucleus of $I = 1/2$, approximately 5% abundant, which we identify as ^{29}Si (Fig. 5). The hyperfine interaction strengths $A_{1,2,3} = 98.24$, 98.13, 94.47 MHz are remarkably similar to the DFT-calculated values (87, 89, 92 MHz, respectively) and directions. A similar case is found for the nitrogen hyperfine, where the experimentally measured values are within 0.3° of the DFT-calculated values. When taken in conjunction with the dopant and treatment history of sample G, these data are enough to conclusively assign the observed spectrum to the defect SiVN (Fig 6).

Comparison of the spin Hamiltonian tensors shows that the hyperfine and g tensors retain the monoclinic symme-

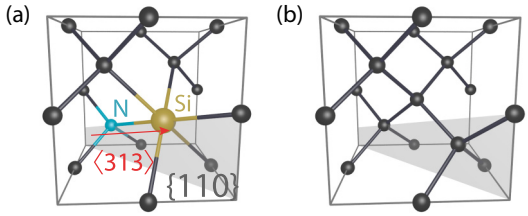

FIG. 6. (a) Schematic of the $SiVN^{0/-}$ defect, highlighting the defect's {1 1 0} mirror plane and the ⟨3 1 3⟩ direction between the nitrogen and silicon atoms. (b) Defect-free region of the diamond lattice for comparison.

try of the defect geometry (Table III). Using the standard approach to hyperfine analysis [72], we may make estimates of the unpaired electron spin density probability. Approximating the ^{29}Si interaction as an axial, dipolar interaction, we obtain isotropic and anisotropic components of 96.9 and −1.24 MHz, respectively. By comparison with tabulated values for 100% localization [73], this corresponds to an approximate unpaired electron spin density probability of 3% on the silicon. In conjunction with a negligible localization on the nitrogen, we conclude the majority of the localization is on the nearest-neighbor carbons, as expected from the DFT-computed wave function [22]. Unfortunately, signal-to-noise limitations mean we have not been able to identify the 1.1% ^{13}C signal associated with these neighbors.

The expected charge state of SiVN can be calculated from the group theoretical descriptions of the SiV defects. Here the neutral and negatively charged SiV defects possess two and one hole, respectively [54]. In replacing one of the neighboring carbon atoms with nitrogen the number of holes present in the defect must decrease by one: we thus expect the positive, neutral and negative charge states to possess 2 ($S = 0$ or 1), 1 ($S = 1/2$), and 0 ($S = 0$) holes. respectively, and we identify the new spectrum with $SiVN^0$. Charge transfer measurements on all samples are consistent with this description. The EPR spectrum is photochromic, with the concentration changing from approximately 400 to <5 ppb between the UV and heat-treated charge states in sample F: the behavior of the defect is therefore qualitatively similar to the behavior of SiV^0. In the heated sample state, we observe no additional EPR spectra and deduce the dominant charge state is $SiVN^-$, which is $S = 0$ in its ground state and therefore EPR inactive.

TABLE IV. Binding energies (E_{bind}, see Sec. III B) for each modeled defect through charge-conserving reactions. Displayed errors result from comparing values calculated using LDA and GGA functional.

Defect	Components	E_{bind} (eV)
$SiVN^0$	$SiV^- + N_s^+$	2.8 ± 0.01
$SiVN^-$	$SiV^- + N_s^0$	4.4 ± 0.1
$SiVN^{2-}$	$SiV^{2-} + N_s^0$	1.8 ± 0.03

DFT calculations of the stability of different charge states of SiV and SiVN are consistent with the observed charge state behavior: the neutral charge states of both defects are stable at approximately the same chemical potential, while $SiVN^-$ is the stable charge state over almost all other chemical potentials [Fig. 7(a)]. These calculations also predict that a double negatively charged SiVN state can exist for high chemical potentials: this charge state would have one hole ($S = 1/2$) and is able to form due to a disruption to the atomic configuration. Structurally, SiVN can be compared to a SiV system with a nitrogen donor and therefore $SiVN^-$ presents an electronically saturated system, as discussed above. DFT calculations indicate that the addition of an extra electron to $SiVN^-$, producing $SiVN^{2-}$, breaks a C-N bond with the nitrogen effectively forming a N_s structure bonded to the Si and two nearest-neighbor carbons. This geometric distortion to SiVN results in the lowering of a band gap state which is now accessible for excitation. Examining the orbital characteristics depicted by spin density isosurfaces from DFT, we observe the N_s^0 -like [Fig. 7(b)] configuration adopted by $SiVN^{2-}$ [Fig. 7(c)], rather than retaining the configuration of the same band gap state in $SiVN^0$ [Fig. 7(d)]. Calculations of the SiVN charge stabilities (Table IV) indicate that all three

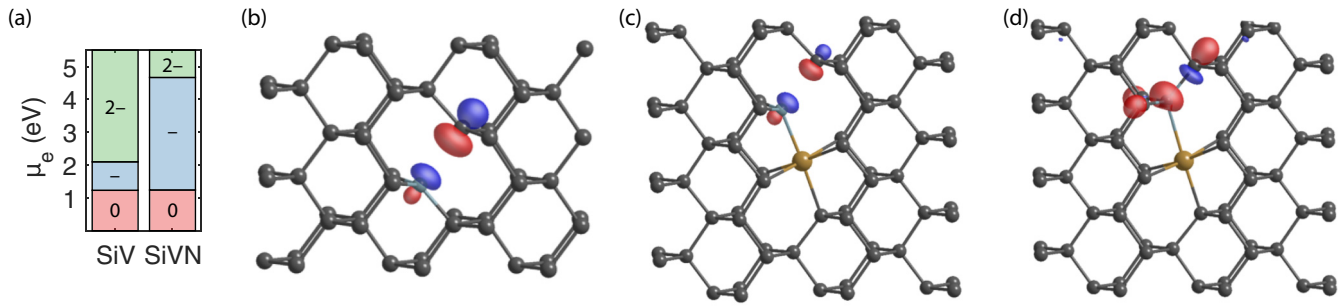

FIG. 7. (a) Schematic of the $SiVN^{0/-}$ defect, highlighting the defect's ⟨1 1 0⟩ mirror plane. (b) Calculated formation energies at varying chemical potentials μ_e for SiV and SiVN with reference to the intrinsic diamond valence band maximum. Transition levels include charge density offset and Madelung corrections. The calculated conduction band minimum was at 4.27 eV. (c)–(e) Electron density on band gap states for (c) the donor state in N_s^0; (d) the state with an unpaired electron for $SiVN^{2-}$; and (e) the same state for $SiVN^0$. Comparison of (d) and (e) highlights the additional electron in an N-C antibonding orbital in $SiVN^{2-}$. Isosurfaces depict a surface of constant spin density: a common spin density threshold was chosen for (d) and (e) to allow comparison in the same structure; a higher threshold was chosen for (c) due to the highly localized nature of the N_s^0 donor state.

charge states are stable configurations, and of these $SiVN^-$ is least likely to dissociate.

We expect all charge states of the SiVN to be difficult to identify in IR absorption measurements. The mass of the elements involved, combined with the vacancy, suggests that defect vibrations will be below the 1332 cm^{-1} lattice cutoff and therefore will contribute to the one-phonon absorption, rather than exhibiting sharp local vibrational modes. Unfortunately, the one-phonon IR absorption of samples D–G contain other unidentified contributions thus no spectrum can be associated with any charge state of SiVN at the present time.

B. Defect production

The addition of silicon (typically via silane) during CVD growth of diamond yields a grown-in (native) population of SiV centers [74,75]. In an analogous situation to nitrogen, where substitutional nitrogen concentrations are typically orders of magnitude higher than the grown-in NV concentrations [76], we presume the majority of the silicon is incorporated as substitutional silicon [16], as discussed in Sec. IV A. Therefore, there is a substantial source of silicon available within the sample itself from growth.

We have not identified $SiVN^0$ in any as-grown samples (putting an upper limit on the as-grown concentration of approximately 0.5 ppb). We first observe $SiVN^0$ upon HPHT annealing at 2000 °C (for 1 h, or 100 h at 1800 °C), and its concentration increases up to the maximum 2400 °C temperature (Fig. 1). As is typical for vacancy-containing defects in diamond, we assume SiVN production must occur via vacancy-assisted migration of impurities, as the energy required for direct diffusion of substitutional nitrogen (8 eV [77]) and silicon is significantly higher than the vacancy-assisted mechanisms [78]. Furthermore, the diffusion barrier for NV^- (≈5 eV [79]) is significantly lower than for SiV^0 (≈6.5 eV [22,54]). At high temperatures where NV is unstable, nitrogen may diffuse through the lattice by concerted exchange with a vacancy before the NV pair breaks up [79]. We therefore understand SiVN production to occur via the diffusion of vacancies and subsequent capture by Si_s, producing SiV; and the vacancy-assisted diffusion of nitrogen to SiV centers producing SiVN.

Recent reports of delayed luminescence at 499 nm from synthetic, silicon-containing samples suggested that the emission originates at Si_xN_y or Si_xN_yV complexes [80]. The 499 nm luminescence is maximized on annealing at 1700 °C and destroyed above 2000 °C [80]. We do not observe this luminescence from any of the present samples at any annealing temperature. Additionally, the annealing behavior of SiVN is incompatible with the reported annealing behavior of the 499 nm defect and therefore we conclude that the luminescence does not originate at SiVN. Furthermore, as SiVN is the simplest variant of the Si_xN_yV defects, and defect aggregation in diamond typically develops from simple to more complex under higher annealing temperatures, it seems unlikely that the emission originates with any defect in this group.

VI. CONCLUSION

The present samples, while dominated in total concentration by nitrogen-related defects, enable additional insight into silicon-related defects and processes which must occur even in lower-concentration samples. The first observation of a doubly charged defect in diamond leads the way for future studies of other doubly charged donors or acceptors, provided the $(+/2+)$ or $(-/2-)$ levels are sufficiently deep.

The existence of SiV^{2-} puts limits on the production efficiency of SiV^- qubits in nitrogen-doped material. Previous reports which interpreted the absence of SiV^- in *n*-type material as the presence of SiV^0 should now be reinterpreted in terms of charge transfer between SiV^{2-} and SiV^-, rather than SiV^0 and SiV^- [81]. As UV light is expected to be required to directly ionize SiV^{2-} it is not clear that it will be possible to design a simple optical ionization protocol to drive $SiV^{2-} \rightarrow SiV^-$—any pulse which ionizes SiV^{2-} is likely also to drive charge in other proximal defects, reducing overall charge stability of the ensemble. Devices which require SiV^- as the dominant charge state should therefore be intrinsic or only moderately *n* type to avoid interference from SiV^{2-} .

ACKNOWLEDGMENTS

We are grateful to Ben Truscott (Element Six) for growing the samples, to John Freeth & Hugh Leach (De Beers Group Technology) for preparing and polishing the samples, to Thoufieq Shaik for initial investigations (De Beers Group Technology), and to David Hardeman (Element Six) for annealing the samples. We thank Andrew Edmonds (Element Six) for careful reading of the manuscript. We acknowledge use of Spectroscopy Research Technology Platform facilities at the University of Warwick. B.L.G. acknowledges funding from the Royal Academy of Engineering. M.E.N. acknowledges funding from EPSRC (Grants No. EP/L015315/1 and No. EP/M013243/1).

[1] M. Atatüre, D. Englund, N. Vamivakas, S.-Y. Lee, and J. Wrachtrup, Nat. Rev. Mater. **3**, 38 (2018).
[2] I. Aharonovich and E. Neu, Adv. Opt. Mater. **2**, 911 (2014).
[3] T. Schröder, S. L. Mouradian, J. Zheng, M. E. Trusheim, M. Walsh, E. H. Chen, L. Li, I. Bayn, and D. Englund, J. Opt. Soc. Am. B **33**, B65 (2016).
[4] D. D. Awschalom, R. Hanson, J. Wrachtrup, and B. B. Zhou, Nat. Photon. **12**, 516 (2018).
[5] M. W. Doherty, N. B. Manson, P. Delaney, F. Jelezko, J. Wrachtrup, and L. C. L. Hollenberg, Phys. Rep. **528**, 1 (2013).
[6] R. E. Evans, M. K. Bhaskar, D. D. Sukachev, C. T. Nguyen, A. Sipahigil, M. J. Burek, B. Machielse, G. H. Zhang, A. S. Zibrov, E. Bielejec, H. Park, M. Lončar, and M. D. Lukin, Science **362**, 662 (2018).
[7] B. C. Rose, D. Huang, Z.-H. Zhang, P. Stevenson, A. M. Tyryshkin, S. Sangtawesin, S. Srinivasan, L. Loudin, M. L. Markham, A. M. Edmonds, D. J. Twitchen, S. A. Lyon, and N. P. de Leon, Science **361**, 60 (2018).
[8] B. L. Green, S. Mottishaw, B. G. Breeze, A. M. Edmonds, U. F. S. D'Haenens-Johansson, M. W. Doherty, S. D. Williams,

D. J. Twitchen, and M. E. Newton, Phys. Rev. Lett. **119**, 096402 (2017).
[9] T. Iwasaki, Y. Miyamoto, T. Taniguchi, P. Siyushev, M. H. Metsch, F. Jelezko, and M. Hatano, Phys. Rev. Lett. **119**, 253601 (2017).
[10] M. E. Trusheim, N. H. Wan, K. C. Chen, C. J. Ciccarino, J. Flick, R. Sundararaman, G. Malladi, E. Bersin, M. Walsh, B. Lienhard, H. Bakhru, P. Narang, and D. Englund, Phys. Rev. B **99**, 075430 (2019).
[11] A. M. Zaitsev, *Optical Properties of Diamond* (Springer, Berlin, 2001).
[12] B. Dischler, *Handbook of Spectral Lines in Diamond* (Springer, Berlin, 2012).
[13] J. P. Goss, R. Jones, S. J. Breuer, P. R. Briddon, and S. Öberg, Phys. Rev. Lett. **77**, 3041 (1996).
[14] L. J. Rogers, K. D. Jahnke, M. W. Doherty, A. Dietrich, L. P. McGuinness, C. Müller, T. Teraji, H. Sumiya, J. Isoya, N. B. Manson, and F. Jelezko, Phys. Rev. B **89**, 235101 (2014).
[15] C. Hepp, T. Müller, V. Waselowski, J. N. Becker, B. Pingault, H. Sternschulte, D. Steinmüller-Nethl, A. Gali, J. R. Maze, M. Atatüre, and C. Becher, Phys. Rev. Lett. **112**, 036405 (2014).
[16] U. F. S. D'Haenens-Johansson, A. M. Edmonds, B. L. Green, M. E. Newton, G. Davies, P. M. Martineau, R. U. A. Khan, and D. J. Twitchen, Phys. Rev. B **84**, 245208 (2011).
[17] B. L. Green, M. W. Doherty, E. Nako, N. B. Manson, U. F. S. D'Haenens-Johansson, S. D. Williams, D. J. Twitchen, and M. E. Newton, Phys. Rev. B **99**, 161112(R) (2019).
[18] K. Iakoubovskii, A. Stesmans, K. Suzuki, J. Kuwabara, and A. Sawabe, Diam. Relat. Mater. **12**, 511 (2003).
[19] A. M. Edmonds, M. E. Newton, P. M. Martineau, D. J. Twitchen, and S. D. Williams, Phys. Rev. B **77**, 245205 (2008).
[20] U. F. S. D'Haenens-Johansson, A. M. Edmonds, M. E. Newton, J. P. Goss, P. R. Briddon, J. M. Baker, P. M. Martineau, R. U. A. Khan, D. J. Twitchen, and S. D. Williams, Phys. Rev. B **82**, 155205 (2010).
[21] V. Nadolinny, A. Komarovskikh, Y. Palyanov, I. Kupriyanov, Y. Borzdov, M. Rakhmanova, O. Yuryeva, and S. Veber, Phys. Status Solidi Appl. Mater. Sci. **213**, 2623 (2016).
[22] J. P. Goss, P. R. Briddon, and M. J. Shaw, Phys. Rev. B **76**, 075204 (2007).
[23] G. Thiering and A. Gali, Phys. Rev. B **92**, 165203 (2015).
[24] R. U. A. Khan, P. M. Martineau, B. L. Cann, M. E. Newton, and D. J. Twitchen, J. Phys.: Condens. Matter **21**, 364214 (2009).
[25] R. U. A. Khan, B. L. Cann, P. M. Martineau, J. Samartseva, J. J. P. Freeth, S. J. Sibley, C. B. Hartland, M. E. Newton, H. K. Dhillon, and D. J. Twitchen, J. Phys.: Condens. Matter **25**, 275801 (2013).
[26] J.-M. Mäki, F. Tuomisto, A. Varpula, D. Fisher, R. U. A. Khan, and P. M. Martineau, Phys. Rev. Lett. **107**, 217403 (2011).
[27] M. W. Dale, Ph.D. thesis, University of Warwick, 2015.
[28] B. L. Green, B. G. Breeze, and M. E. Newton, J. Phys.: Condens. Matter **29**, 225701 (2017).
[29] G. Davies, Phys. B Condens. Matter **273–274**, 15 (1999).
[30] M. J. Rayson and P. R. Briddon, Phys. Rev. B **80**, 205104 (2009).
[31] J. P. Perdew, K. Burke, and M. Ernzerhof, Phys. Rev. Lett. **77**, 3865 (1996).
[32] C. Hartwigsen, S. Gœdecker, and J. Hutter, Phys. Rev. B **58**, 3641 (1998).
[33] H. J. Monkhorst and J. D. Pack, Phys. Rev. B **13**, 5188 (1976).
[34] D. P. Riley, Nature (London) **153**, 587 (1944).
[35] J. P. Goss, P. R. Briddon, R. Jones, and S. Sque, Diam. Relat. Mater. **13**, 684 (2004).
[36] S. B. Zhang and J. E. Northrup, Phys. Rev. Lett. **67**, 2339 (1991).
[37] J. Shim, E.-K. Lee, Y. J. Lee, and R. M. Nieminen, Phys. Rev. B **71**, 035206 (2005).
[38] J. P. Goss and P. R. Briddon, Phys. Rev. B **77**, 035211 (2008).
[39] M. J. Shaw, P. R. Briddon, J. P. Goss, M. J. Rayson, A. Kerridge, A. H. Harker, and A. M. Stoneham, Phys. Rev. Lett. **95**, 105502 (2005).
[40] G. S. Woods, J. A. Van Wyk, and A. T. Collins, Philos. Mag. B **62**, 589 (1990).
[41] S. C. Lawson, D. Fisher, D. C. Hunt, and M. E. Newton, J. Phys.: Condens. Matter **10**, 6171 (1998).
[42] S. Liggins, Ph.D. thesis, University of Warwick, 2010.
[43] C. Glover, M. E. Newton, P. Martineau, D. J. Twitchen, and J. M. Baker, Phys. Rev. Lett. **90**, 185507 (2003).
[44] C. B. Hartland, Ph.D. thesis, University of Warwick, 2014.
[45] T. Evans and Z. Qi, Proc. R. Soc. London Ser. A **381**, 159 (1982).
[46] W. Wang, M. S. Hall, K. S. Moe, J. Tower, and T. M. Moses, Gems Gemol. **43**, 294 (2007).
[47] R. U. A. Khan, P. M. Martineau, B. L. Cann, M. E. Newton, H. K. Dhillon, and D. J. Twitchen, Gems Gemol. **46**, 18 (2010).
[48] Y. Palyanov, I. Kupriyanov, Y. Borzdov, D. Nechaev, and Y. Bataleva, Crystals **7**, 119 (2017).
[49] Y. N. Palyanov, I. N. Kupriyanov, Y. M. Borzdov, and Y. V. Bataleva, CrystEngComm **17**, 7323 (2015).
[50] P. Martineau, S. C. Lawson, A. J. Taylor, S. J. Quinn, D. J. F. Evans, and M. Crowder, Gems Gemol. **40**, 2 (2004).
[51] S. Häußler, G. Thiering, A. Dietrich, N. Waasem, T. Teraji, J. Isoya, T. Iwasaki, M. Hatano, F. Jelezko, A. Gali, and A. Kubanek, New J. Phys. **19**, 063036 (2017).
[52] E. A. Ekimov, V. S. Krivobok, S. G. Lyapin, P. S. Sherin, V. A. Gavva, and M. V. Kondrin, Phys. Rev. B **95**, 094113 (2017).
[53] E. A. Ekimov, P. S. Sherin, V. S. Krivobok, S. G. Lyapin, V. A. Gavva, and M. V. Kondrin, Phys. Rev. B **97**, 045206 (2018).
[54] A. Gali and J. R. Maze, Phys. Rev. B **88**, 235205 (2013).
[55] G. D. Watkins, Mater. Sci. Semicond. Process. **3**, 227 (2000).
[56] R. C. Newman, Rep. Prog. Phys. **45**, 1163 (1982).
[57] J. R. Weber, A. Janotti, and C. G. Van De Walle, Phys. Rev. B **87**, 035203 (2013).
[58] J. R. Weber, A. Janotti, and C. G. Van de Walle, in *Photonics and Electronics with Germanium*, 1st ed., edited by K. Wada and L. C. Kimerling (Wiley-VCH, Berlin, 2015).
[59] S. J. Breuer and P. R. Briddon, Phys. Rev. B **51**, 6984 (1995).
[60] A. Mainwood and A. M. Stoneham, J. Phys.: Condens. Matter **9**, 2453 (1997).
[61] G. D. Watkins and J. R. Troxell, Phys. Rev. Lett. **44**, 593 (1980).
[62] R. G. Farrer, Solid State Commun. **7**, 685 (1969).
[63] R. Jones, J. P. Goss, and P. R. Briddon, Phys. Rev. B **80**, 033205 (2009).
[64] M. Kern, J. Jeske, D. W. Lau, A. D. Greentree, F. Jelezko, and J. Twamley, Phys. Rev. B **95**, 235306 (2017).
[65] B. L. Green, M. W. Dale, M. E. Newton, and D. Fisher, Phys. Rev. B **92**, 165204 (2015).

[66] W. Smith, P. Sorokin, I. Gelles, and G. Lasher, Phys. Rev. **115**, 1546 (1959).
[67] J. H. N. Loubser and J. A. van Wyk, Diam. Res. **11**, 11 (1977).
[68] J. H. N. Loubser and J. A. van Wyk, Rep. Prog. Phys. **41**, 1201 (1978).
[69] S. Felton, B. L. Cann, A. M. Edmonds, S. Liggins, R. J. Cruddace, M. E. Newton, D. Fisher, and J. M. Baker, J. Phys.: Condens. Matter **21**, 364212 (2009).
[70] V. A. Nadolinny, A. P. Yelisseyev, J. M. Baker, D. J. Twitchen, M. E. Newton, A. Hofstaetter, and B. Feigelson, Phys. Rev. B **60**, 5392 (1999).
[71] S. Stoll and A. Schweiger, J. Magn. Reson. **178**, 42 (2006).
[72] C. G. Van de Walle and P. E. Blöchl, Phys. Rev. B **47**, 4244 (1993).
[73] J. R. Morton and K. F. Preston, J. Magn. Reson. **30**, 577 (1978).
[74] K. M. Itoh and H. Watanabe, MRS Commun. **4**, 143 (2014).
[75] L. J. Rogers, K. D. Jahnke, T. Teraji, L. Marseglia, C. Müller, B. Naydenov, H. Schauffert, C. Kranz, J. Isoya, L. P. McGuinness, and F. Jelezko, Nat. Commun. **5**, 4739 (2014).
[76] A. M. Edmonds, U. F. S. D'Haenens-Johansson, R. J. Cruddace, M. E. Newton, K.-M. C. Fu, C. Santori, R. G. Beausoleil, D. J. Twitchen, and M. L. Markham, Phys. Rev. B **86**, 035201 (2012).
[77] J. P. Goss and P. R. Briddon, Phys. Rev. B **73**, 085204 (2006).
[78] A. Mainwood, Phys. Rev. B **49**, 7934 (1994).
[79] H. Pinto, R. Jones, D. W. Palmer, J. P. Goss, P. R. Briddon, and S. Öberg, Phys. Status Solidi **209**, 1765 (2012).
[80] A. M. Wassell, C. D. McGuinness, C. Hodges, P. M. Lanigan, D. Fisher, P. M. Martineau, M. E. Newton, and S. A. Lynch, Phys. Status Solidi Appl. Mater. Sci. **215**, 1800292 (2018).
[81] S. Dhomkar, P. R. Zangara, J. Henshaw, and C. A. Meriles, Phys. Rev. Lett. **120**, 117401 (2018).